J. Fluid Mech. (2008), *vol.* 606, *pp.* 209–223.
doi:10.1017/S0022112008001663 Printed in the United Kingdom

Dynamics of axisymmetric bodies rising along a zigzag path

PEDRO C. FERNANDES, PATRICIA ERN, FRÉDÉRIC RISSO AND JACQUES MAGNAUDET

Institut de Mécanique des Fluides, UMR 5502 CNRS-INP-UPS
Allée du Prof. Camille Soula, 31400 Toulouse, France

(Received 5 September 2006 and in revised form 20 March 2008)

The forces and torques governing the planar zigzag motion of thick, slightly buoyant disks rising freely in a liquid at rest are determined by applying the generalized Kirchhoff equations to experimental measurements of the body motion performed for a single body-to-fluid density ratio $\rho_s/\rho_f \approx 1$. The evolution of the amplitude and phase of the various contributions is discussed as a function of the two control parameters, i.e. the body aspect ratio (the diameter-to-thickness ratio $\chi = d/h$ ranges from 2 to 10) and the Reynolds number ($100 < Re < 330$), Re being based on the rise velocity and diameter of the body. The body oscillatory behaviour is found to be governed by the force balance along the transverse direction and the torque balance. In the transverse direction, the wake-induced force is mainly balanced by two forces that depend on the body inclination, i.e. the inertia force generated by the body rotation and the transverse component of the buoyancy force. The torque balance is dominated by the wake-induced torque and the restoring added-mass torque generated by the transverse velocity component. The results show a major influence of the aspect ratio on the relative magnitude and phase of the various contributions to the hydrodynamic loads. The vortical transverse force scales as $f_o = (\rho_f - \rho_s)gh\pi d^2$ whereas the vortical torque involves two contributions, one scaling as $f_o d$ and the other as $f_1 d$ with $f_1 = \chi f_o$. Using this normalization, the amplitudes and phases of the vortical loads are made independent of the aspect ratio, the amplitudes evolving as $(Re/Re_{c1} - 1)^{1/2}$, where Re_{c1} is the threshold of the first instability of the wake behind the corresponding body held fixed in a uniform stream.

1. Introduction

Determining the forces and torques at the origin of any motion is a long-standing *raison d'être* of mechanics. While a large number of results is available for hydrodynamic forces acting on fixed bodies or on bodies with a prescribed rectilinear motion, much less is known for loads experienced by freely moving bodies driven by an external force, such as gravity. The central difficulty is tied to the intrinsic coupling between the fluid and body motions, the relative body displacement inducing a disturbance in the fluid which in turn imposes loads that govern the body motion. Also, the governing equations and the interpretation of the hydrodynamic couplings between the various degrees of freedom become significantly more complex as soon as the body exhibits some geometrical anisotropy and starts rotating. From an experimental viewpoint, accurately following the body motion is

a non-trivial task, even with modern means, and describing the body kinematics is a crucial part of the investigation. Despite these various difficulties, predicting the hydrodynamic loads on such freely moving bodies as a function of the body geometry and the characteristic parameters of the fluid/body system is of primary importance in many applications ranging from aerodynamics (Lugt 1983) to biomechanics (Wang 2005) and dispersed two-phase flows (Magnaudet & Eames 2000), to mention just a few. This is why this topic has become an active field of research in recent years.

The general motion of a rigid body in an inviscid fluid at rest at infinity is governed by the Kirchhoff equations (Lamb 1932). Generic theoretical and computational investigations have considered the possible rational generalization of these equations to finite-Reynolds-number flows. These studies converged to the key result that the so-called added-mass effects due to the instantaneous displacement of the fluid induced by any relative acceleration of the body are unaffected by viscous effects and can be isolated from the wake-induced effects resulting from vorticity generation at the body surface (see Howe 1995; Magnaudet & Eames 2000; Mougin & Magnaudet 2002*a* and references therein). Using this result, Mougin & Magnaudet (2002*b*) solved numerically the coupled fluid/body problem for a freely rising spheroidal bubble with a prescribed shape, determining the fluid motion through the solution of the full Navier–Stokes equations and the body motion through that of the generalized Kirchhoff equations. They subsequently processed their numerical data to determine the wake-induced forces and torques acting on the bubble when it moves along a planar zigzag followed by a circular helical path (Mougin & Magnaudet 2006) and showed how the time evolution of these vortical loads is connected to that of the wake structure.

In experiments, the vortical wake-induced loads acting on the body cannot be directly determined. However, the body motion can be accurately measured by means of imaging techniques. Provided the body- and added-inertia tensors are known, the projections of the buoyancy and inertia loads onto axes rotating with the body can thus be determined using the body kinematics. Then, the vortical loads are straightforwardly obtained through the balances provided by the generalized Kirchhoff equations. Andersen, Pesavento & Wang (2005) took advantage of this to determine the loads acting on a two-dimensional freely falling plate in four particular cases of fluttering, tumbling and irregular paths. Shew, Poncet & Pinton (2006) used the same procedure to evaluate the vortical force and torque acting on spheroidal bubbles along their zigzag/helical path.

Following the same methodological line, our purpose in the present work is to determine how the various loads acting on an axisymmetric body (which may be considered either as a 'thin cylinder' or a 'thick disk') evolve when one of the control parameters, namely the body aspect ratio, is varied continuously over a wide range within which the body mainly follows a quasi-planar zigzag motion. Hence, in contrast to the recent investigations mentioned above in which several widely separated sets of parameters were selected to shed light on various path transitions, we focus instead on a single type of path but try to understand how the various loads (and hence the wake-induced effects) scale with the aspect ratio and, to some extent, with the Reynolds number. Our goal is to provide a detailed set of information which, combined with those offered in the available studies reviewed above, including those devoted to spheroidal bubbles, can guide the development of rational and general models for the wake-induced loads.

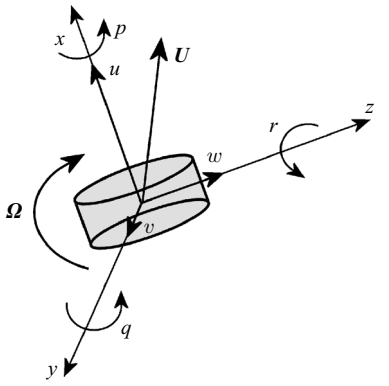

FIGURE 1. Sketch of the rotating axes (x,y,z) and definition of the components of the velocity $\boldsymbol{U}$ and rotation rate $\boldsymbol{\Omega}$ of the body.

We consider disks of various thicknesses (sketched in figure 1), so that the problem is governed by three dimensionless parameters

$$\chi = \frac{d}{h}, \quad Re = \frac{V\,d}{\nu} \quad \text{and} \quad \frac{\rho_s}{\rho_f}, \tag{1.1}$$

where χ denotes the body aspect ratio, d its diameter and h its thickness. In the Reynolds number Re, V stands for the body vertical velocity and ν for the liquid kinematic viscosity. The last parameter, the ratio of the body-to-fluid densities ρ_s/ρ_f, is set to a fixed value very close to 1. In contrast, χ and Re are varied in the range $2 < \chi < 10$ and $100 < Re < 330$, respectively. Both parameters are expected to have a significant influence on the loads acting on the body. On the one hand, the Reynolds number modifies the strength of the vortical effects on the body but does not affect the proper and added-fluid coefficients in the inertia terms. On the other hand, inertia terms strongly depend on the geometrical anisotropy of the body and thus vary with χ. The body aspect ratio may also be expected to influence the relative magnitude of the vortical loads on the body along its axial and transverse directions. Moreover, we recently showed (Fernandes *et al.* 2005) that, independently of the specific body shape (cylindrical or spheroidal), the aspect ratio strongly modifies the way a body evolves along its periodic zigzag path: the oscillations of the orientation and those of the velocity are nearly in phase for thick bodies ($\chi \leqslant 3$), resulting in a style of motion in which the body axis is almost aligned with the tangent to the path, whereas they are more than $\pi/2$ out of phase for thin bodies ($\chi \geqslant 8$), so that such bodies mainly slide along the path with their midplane aligned with its tangent. It is therefore of central importance to understand how the variations of the contributions to the force and torque balances are capable of supporting such contrasting motions.

The present paper makes use of the kinematic characteristics of the body motion obtained and discussed in Fernandes *et al.* (2007) to which the reader is referred for details concerning the experiments and data processing. Section 2 presents the generalized Kirchhoff equations and how they simplify according to the experimental observations. The various contributions to the force and torque balances are described in § 3 as a function of the governing parameters and the dominant terms in each projection of these balances are determined and discussed. This section also provides comparisons with similar results available for a spheroidal bubble and the two-dimensional flat plate. The modelling of the oscillatory vortical efforts is addressed in

§ 4 where the general scaling of F_ω^y and Γ_ω^z is established and yields the basis of an empirical model.

2. Equations of motion

The motion of a non-deformable body through an unbounded viscous fluid at rest at infinity is governed by the generalized Kirchhoff equations (Howe 1995; Mougin & Magnaudet 2002*a*), which express the linear and angular momentum balances for the complete fluid/body system. These equations are commonly written in a system of axes with origin fixed with respect to the observer and axes rotating with the body (say, x directed along the body symmetry axis and (y, z) along two perpendicular radial directions, as shown in figure 1). For uniform fluid and body densities, they are

$$(m\mathbb{I} + \mathbb{A})\cdot\frac{\mathrm{d}\boldsymbol{U}}{\mathrm{d}t} + \boldsymbol{\Omega} \times ((m\,\mathbb{I} + \mathbb{A})\cdot\boldsymbol{U}) = \boldsymbol{F}_\omega + \boldsymbol{F}_g, \tag{2.1}$$

$$(\mathbb{J} + \mathbb{D})\cdot\frac{\mathrm{d}\boldsymbol{\Omega}}{\mathrm{d}t} + \boldsymbol{\Omega} \times ((\mathbb{J} + \mathbb{D})\cdot\boldsymbol{\Omega}) + \boldsymbol{U} \times (\mathbb{A}\cdot\boldsymbol{U}) = \boldsymbol{\Gamma}_\omega, \tag{2.2}$$

where $\boldsymbol{U}$ is the velocity of the centre of mass of the body and $\boldsymbol{\Omega}$ its rotation rate. The left-hand side of (2.1)–(2.2) contains the inertia terms associated with the body (of mass m and inertia tensor $\mathbb{J}$, $\mathbb{I}$ being the unit tensor), and those due to the fluid set in motion instantaneously by a translational or a rotational acceleration of the body (characterized by the second-order diagonal tensors $\mathbb{A}$ and $\mathbb{D}$, respectively). The latter terms will be referred to as added-mass or added-inertia loads in what follows. On the right-hand side of (2.1)–(2.2), $\boldsymbol{F}_g$ stands for the buoyancy force and $\boldsymbol{F}_\omega$ and $\boldsymbol{\Gamma}_\omega$ are the entire force and torque resulting from the existence of vorticity in the flow, due to vorticity generation at the body surface (in particular, they contain possible history effects). The latter contributions will be referred to as the vortical force and torque, respectively. It is now established that added-mass effects are not affected by vorticity and have coefficients independent of the flow characteristics (in particular the Reynolds number) and of the boundary condition at the body surface and hence of the wake structure (see Magnaudet & Eames 2000 and Mougin & Magnaudet 2002*a* and references therein). Therefore, knowing the body geometry, $\mathbb{A}$ and $\mathbb{D}$ can be computed as if the flow were irrotational. This is how the separation between added-mass and vortical hydrodynamic loads is achieved unambiguously in (2.1)–(2.2).

Let (u, v, w) and (p, q, r) be the components of $\boldsymbol{U}$ and $\boldsymbol{\Omega}$ in the rotating axes (x, y, z) shown in figure 1. A major simplification to the system (2.1)–(2.2) arises from the fact that no significant rotation p of the body about its symmetry axis was observed experimentally (Fernandes *et al.* 2007). This eliminates the torque equation along the x-direction and allows us to decouple the inertia terms in (2.1)–(2.2) for the translational and angular velocities in the diametrical plane (y, z). Moreover, in most cases, the body path is nearly a vertical zigzag lying in the (x, y)-plane, since we determined $w < 0.35\,v$ and $q < 0.35\,r$. Thus, the cross-product involving w and q in (2.1) provides a negligible contribution to the force balance along the axial direction and the equations for w and q are the same as those for v and r, but with lower amplitudes. Therefore (2.1)–(2.2) can be reduced to a system of three equations governing the velocity components u and v and the rotation rate $r = \mathrm{d}\theta/\mathrm{d}t$, θ being the inclination angle between the body symmetry axis x and the vertical direction.

We are then left with

$$\left(\frac{\rho_s}{\chi\rho_f}+A\right)\frac{\mathrm{d}u}{\mathrm{d}t}-\left(\frac{\rho_s}{\chi\rho_f}+B\right)vr=F_\omega^x+\cos\theta, \tag{2.3}$$

$$\left(\frac{\rho_s}{\chi\rho_f}+B\right)\frac{\mathrm{d}v}{\mathrm{d}t}+\left(\frac{\rho_s}{\chi\rho_f}+A\right)ur=F_\omega^y-\sin\theta, \tag{2.4}$$

$$\left(\frac{\rho_s}{\chi\rho_f}J_2+Q\right)\frac{\mathrm{d}r}{\mathrm{d}t}-(A-B)\,uv=\Gamma_\omega^z, \tag{2.5}$$

F_ω^x and F_ω^y being the components of the vortical force $\boldsymbol{F}_\omega$ along the x- and y-directions, respectively, while Γ_ω^z is the component of the vortical torque $\boldsymbol{\Gamma}_\omega$ along the z-direction. The above equations are written in dimensionless form using the scales $l_o = d$, $u_o = ((\Delta\rho/\rho_f)gh)^{1/2}$, $f_o = \Delta\rho\vartheta g = \rho_f u_o^2\pi d^2$, for the length, velocity and force, respectively, $\Delta\rho = \rho_f - \rho_s$ being the density difference, ϑ the volume of the body and g denoting gravity. J_2 is the dimensionless moment of inertia of the body about the z-axis, i.e. $J_2 = 1/16 + \chi^{-2}/12$.

Equations (2.3)–(2.5) also involve the added-mass coefficients A and B which correspond to a body acceleration in the axial and transverse directions, respectively, and the added-moment-of-inertia coefficient Q corresponding to a rotation about the z-axis. No exact expression for these coefficients is available for a cylinder of finite thickness. In what follows we use the following approximate expressions:

$$A=\frac{4}{3\pi}(1+0.5\,\chi^{-1/2}),\quad B=\frac{7}{3\pi}\chi^{-7/4},\quad Q=\frac{2}{45\pi}(1+0.8\,\chi^{-1/2}). \tag{2.6}$$

The expressions for A and B were obtained by fitting the numerical results of Loewenberg (1993*a*, *b*, 1994) over the range of χ covered by our experiments. No result for Q seems to be available. Therefore we assumed the above expression, which displays a decrease with χ similar to that of A and matches the asymptotic value $Q = 2/(45\pi)$ known for a flat disk ($\chi \to \infty$). The uncertainty in Q is therefore larger for thicker bodies. However the body moment of inertia J_2 is considerably larger in this case, so that we expect the uncertainty in Q to have little effect on (2.5). Moreover, as will be shown below, it turns out that knowing the exact expression for Q is of little importance since the torque induced by the angular acceleration provides a negligible contribution to (2.5).

Note that as $\rho_s/\rho_f \simeq 1$ and A is much larger than B for $\chi > 1.5$, $(\rho_s/\chi\rho_f + A)$ is larger than $(\rho_s/\chi\rho_f + B)$ which is close to $1/\chi$, and that the prefactor $(A - B)$ in the restoring added-mass torque is much larger than the factor $((\rho_s/\chi\rho_f)J_2 + Q)$ in front of the angular acceleration. Once these coefficients are known, knowledge of the body orientation and velocity allows us to determine the various contributions of inertia and buoyancy acting on the body at any time and to evaluate the unknown vortical force and torque using the balance expressed by (2.3)–(2.5).

3. Analysis of the force and torque balances

For each aspect ratio, provided the Reynolds number is lower than a critical value $Re_c(\chi)$, the body follows a rectilinear path with its symmetry axis aligned with the vertical direction. We then have $u = \overline{u}$, $v = 0$, $\theta = 0$ and the force balance (2.3) reduces to $F_\omega^x = -1$, a steady drag force balancing the buoyancy driving force. For $Re > Re_c(\chi)$, the body follows a periodic zigzag path. For $Re \leqslant 330$ and $2 \leqslant \chi \leqslant 10$, the experimental results revealed that the body orientation and velocity can be

described accurately by

$$u(t) = \overline{u}, \quad v(t) = \widetilde{v}\sin(St - \phi_Y), \quad \theta(t) = \widetilde{\theta}\sin(St), \tag{3.1}$$

where $S = 2\pi f d/u_o$ is the Strouhal number based on the frequency f of the path oscillations and ϕ_Y is the phase lag of v with respect to θ. Both quantities were found to be weakly dependent on the Reynolds number, but strongly dependent on the aspect ratio, since S (resp. ϕ_Y) varies from about 0.6 to 1.9 (resp. from 170° to 230°) when χ varies from 2 to 10.

As u is constant and v and θ oscillate with the same dimensionless frequency S, the inertia terms of (2.3)–(2.5) are also pure harmonic functions. Moreover, the maximum inclination angle $\widetilde{\theta}$ being smaller than 35°, the components of the buoyancy force in the rotating frame can be approximated as

$$\cos\theta \simeq 1 - \tfrac{1}{2}\theta^2 \quad \text{and} \quad \sin\theta \simeq \sin\widetilde{\theta}\sin(St) \simeq \frac{\sin\widetilde{\theta}}{\widetilde{\theta}}\theta. \tag{3.2}$$

Hence it turns out that in the axial direction, equation (2.3) corresponds mainly to a balance between the steady part of the vortical force, say $\overline{F_\omega^x}$, and the steady part of the buoyancy force, resulting in a constant axial velocity $\overline{u}$. The oscillatory behaviour of v and θ only induces a slight modification in this balance ($\overline{F_\omega^x}$ increases from -1 to -0.96 for $Re = 300$, quite independently of the aspect ratio) and the oscillatory part of F_ω^x (at frequency $2S$) is less than 10% (resp. 20%) in amplitude of $\overline{F_\omega^x}$ for $\chi \leqslant 6$ (resp. $\chi > 6$). Therefore, the oscillations of the transverse velocity v and orientation θ are only governed by equations (2.4)–(2.5), which, given (3.1)–(3.2), reduce to the following linear set of coupled equations:

$$\underbrace{\left(\frac{\rho_s}{\chi\rho_f} + B\right)\frac{\mathrm{d}v}{\mathrm{d}t}}_{F_{\dot{v}}} + \underbrace{\left(\frac{\rho_s}{\chi\rho_f} + A\right)\overline{u}r}_{F_{ur}} + \underbrace{\frac{\sin\widetilde{\theta}}{\widetilde{\theta}}\theta}_{F_g} = F_\omega^y. \tag{3.3}$$

$$\underbrace{\left(\frac{\rho_s}{\chi\rho_f}J_2 + Q\right)\frac{\mathrm{d}r}{\mathrm{d}t}}_{\Gamma_{\dot{r}}} \quad \underbrace{-(A-B)\overline{u}v}_{\Gamma_{uv}} = \Gamma_\omega^z. \tag{3.4}$$

The time evolutions of the various forces components acting along the transverse direction of a thick body ($\chi = 2$) and a thin body ($\chi = 10$) are displayed in figure 2 (a, b). It appears that the relative amplitudes and phase lags of the forces follow qualitatively similar evolutions for both aspect ratios; the two force balances are thus qualitatively similar. In contrast, the amplitudes and phase lags of the transverse velocity v display very different evolutions for the two aspect ratios. To better understand this difference, we consider the torque balance. The corresponding time evolutions of the torques $\Gamma_{\dot{r}}$, Γ_{uv} and Γ_ω^z are also shown in figure 2(c, d). It is obvious from these figures that the strength of the various torques strongly increases with the aspect ratio. For instance the vortical torque is found to be about three times larger for $\chi = 10$ than for $\chi = 2$, as is also the case for v, and both quantities appear also to be of opposite phase.

Let us now discuss the effect of the parameters Re and χ on the various contributions to the balances (3.3)–(3.4). The amplitudes of the four terms involved in the transverse force balance increase strongly with Re while their increase with

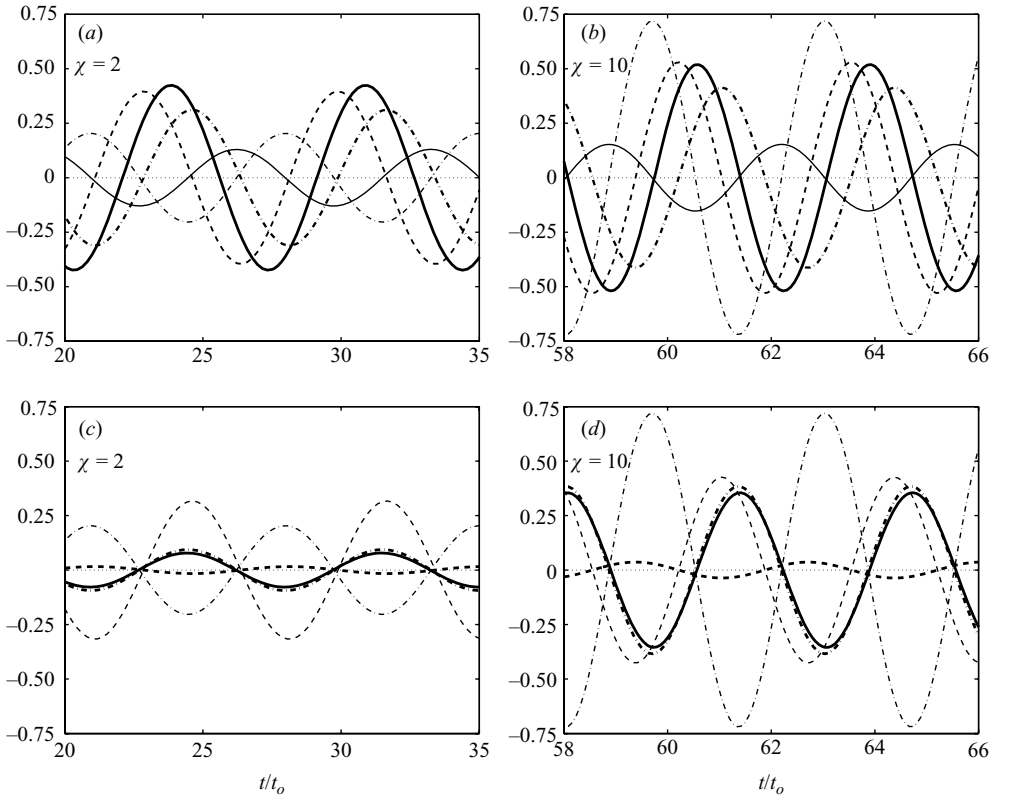

FIGURE 2. (a, b) Time evolution of $F_{\dot{v}}$ (—), F_{ur} (– –), F_g (– · –), F_ω^y (——) and v (— · —) (θ is superimposed on F_g). (c, d) Time evolution of $\Gamma_{\dot{r}}$ (- -), Γ_{uv} (- · -), Γ_ω^z (——), v (— · —) and θ (——). (a, c) Thick body with $\chi = 2$; (b, d) thin body with $\chi = 10$ ($Re = 250$).

χ is weaker. The contribution $F_{\dot{v}}$ corresponding to the time rate-of-change of the transverse velocity is significantly smaller than the other three terms (less than 0.3 for $Re < 330$) and is almost independent of the aspect ratio since the decrease of the prefactor $(\rho_s/\chi\rho_f + B)$ with χ is compensated by the increase of both the frequency S and the amplitude of the transverse motion $\widetilde{v}$. The increase of F_{ur} with χ directly follows that of the rotation rate $\widetilde{r} = \widetilde{\theta}\, S$ and is only partly attenuated by the decrease of the prefactor $(\rho_s/\chi\rho_f + A)$. Hence at a given Re, the variation of the two inertia terms with respect to χ follows a tendency opposite to that of the inertia and added-inertia coefficients. The variation of the amplitude of the buoyancy term F_g with Re and χ follows that of $\widetilde{\theta}$. Consequently, the amplitude of the vortical force F_ω^y increases with χ and even more with Re, as shown in figure 3(a). Note that the increase of the Strouhal number with the aspect ratio reported in Fernandes *et al.* (2007) can now be seen as a consequence of this transverse force balance: taken together, the increase of the transverse component of the vortical force and the decrease of the inertia coefficients with χ require a faster transverse motion.

The amplitudes of the torques $\Gamma_{\dot{r}}$ and Γ_{uv} increase with both the Reynolds number and the aspect ratio. The evolution with Re follows that of the amplitudes of the oscillations of v and θ. The evolution with χ is more subtle since, at a given Re, the effect of the aspect ratio cannot be anticipated on the grounds of the variations of the inertia and added-inertia coefficients. Indeed for $\chi \geqslant 2$, $(A - B)$ depends only slightly

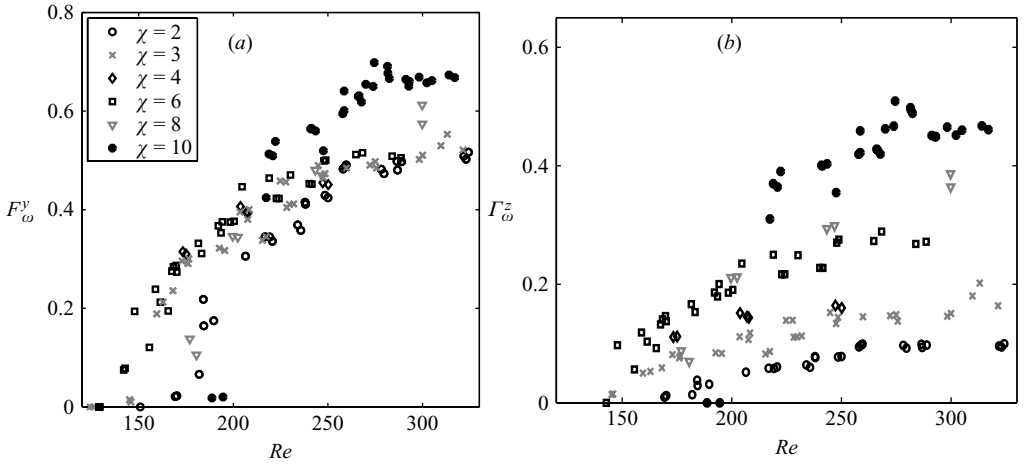

FIGURE 3. Amplitude of the transverse force F^y_ω (a) and of the torque Γ^z_ω (b) as a function of the Reynolds number for various aspect ratios.

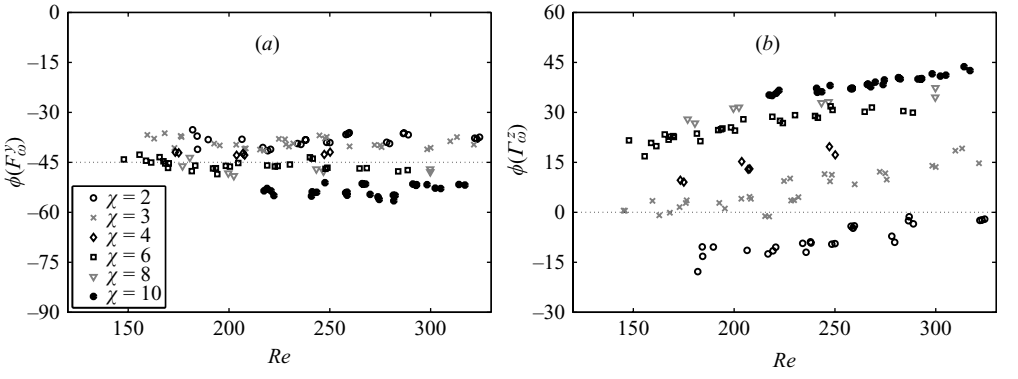

FIGURE 4. Phases relative to θ of F^y_ω (a) and Γ^z_ω (b) as a function of the Reynolds number for various aspect ratios.

on χ while the prefactor $((\rho_s/\chi\rho_f)\,J_2 + Q)$ is a decreasing function of the aspect ratio. The increase of $\Gamma_{\dot{r}}$ with χ is mainly due to that of the oscillation frequency through a factor S^2. Similarly, the increase of the restoring added-mass torque Γ_{uv} follows that of $\widetilde{v}$. It turns out that for all aspect ratios, the amplitude of Γ_{uv} is larger than that of $\Gamma_{\dot{r}}$ by a factor of $O(10)$. As a consequence of the balance (3.4), the variation of the amplitude of the vortical torque Γ^z_ω with χ and Re, which is shown in figure 3(b), is very close to that of Γ_{uv}. Moreover, as Γ_{uv} is of opposite phase to v, the phase $\phi(\Gamma^z_\omega)$ of the vortical torque relative to θ is also opposite to that of v, i.e. $\phi(\Gamma^z_\omega) \simeq \phi_Y - \pi$. Figure 4 reveals that $\phi(\Gamma^z_\omega)$ strongly depends on the aspect ratio, contrasting with its weak sensitivity to the Reynolds number. In contrast, as the phases of F_{ur} and F_g are locked to θ, the phase lag of the transverse vortical force $\phi(F^y_\omega)$ relative to θ depends only slightly on χ and is nearly independent of Re: figure 4 shows that $\phi(F^y_\omega)$ varies from -35° to -55° when χ varies from 2 to 10.

To summarize, the vortical force F^y_ω is mainly balanced by two forces that depend on the body inclination: F_{ur}, the inertia force generated by the body rotation (proportional to the mass of the body plus an added mass of fluid), and the

transverse component of the buoyancy force, F_g. On the other hand, the vortical torque is mainly balanced by the restoring added-mass torque Γ_{uv} associated with the transverse velocity component and the body geometrical anisotropy, the torque associated with the angular acceleration making a negligible contribution. These balances indicate that, although the vortical force and torque presumably depend on both the translational and rotational degrees of freedom of the body, the body rotation (resp. transverse velocity) is essentially regulated by the transverse component of the vortical force (resp. by the vortical torque). In particular, a stronger vortical torque, such as that observed for thin bodies, corresponds to a larger transverse velocity, i.e. a larger angle between the body symmetry axis and the body velocity. The same conclusions were obtained numerically from the force and torque balances governing the zigzag/helical path of an oblate spheroidal bubble (Mougin & Magnaudet 2006). However, the transverse velocity required to balance the vortical torque is much smaller in the case of a bubble since the rise velocity is much larger, owing to the large density difference. In contrast, the axial and transverse force balances reported by Andersen *et al.* (2005) in the case of a fluttering thin two-dimensional plate at $Re = O(10^3)$ and $\rho_s/\rho_f \approx 2.5$ reveal very different equilibria. Under these conditions, nonlinear effects are important and the plate exhibits a periodic motion with noticeable higher-frequency harmonics and with a transverse velocity about three times larger than the mean fall velocity. The transverse linear acceleration of the body then provides a dominant contribution to the transverse force balance, whereas the added-mass terms appear negligible. In addition, the fluctuating and mean drag contributions to the axial force balance are of the same order of magnitude and the associated added-mass contribution is significant.

4. Modelling of the vortical loads

The fact that the amplitudes of the vortical loads at a given Reynolds number are larger for thinner bodies is in line with what happens for fixed bodies. Indeed, numerical simulations of the flow about fixed thick disks (Fernandes *et al.* 2007) revealed that the first two consecutive bifurcations of the wake (associated with a loss of axial symmetry and a loss of stationarity, respectively) arise at critical Reynolds numbers that decrease with the aspect ratio. In the stable regime, i.e. below the first critical Reynolds number, the strength of wake effects (especially that of the attached eddy) can be characterized by the maximum of the reverse velocity in the recirculating region, V_t, which increases with the aspect ratio, and by a Reynolds number $Re^* = V_t d/\nu$ based on it. This modified Reynolds number was found to be related to Re through the simple empirical relation $Re^* = 0.62\chi Re/(1+\chi)$. It then turned out that the two aforementioned wake bifurcations arise at two constant values of Re^*, irrespective of the aspect ratio, namely $Re^*_{c1} \approx 72$ and $Re^*_{c2} \approx 78$. The analysis of the kinematics of freely moving bodies performed by Fernandes *et al.* (2007) also showed that, if the parameter Re^* is introduced, the constant axial velocity scales with the gravitational velocity based on the body thickness, $u_o = ((\Delta\rho/\rho_f)gh)^{1/2}$, while the relevant length and velocity for the path oscillations are the body diameter d and the gravitational velocity based on it, $u_1 = ((\Delta\rho/\rho_f)gd)^{1/2}$. As a consequence, the Strouhal number S is proportional to $u_1/u_o = \chi^{1/2}$. The measurements of the axial velocity, $\overline{u}$, and of the amplitudes of the fluctuations, $\widetilde{v}/S$ and $\widetilde{\theta}$, then fall around master curves independent of χ given by

$$\overline{u} \approx 1.35 - 3.5 \times 10^{-3}(Re^* - Re^*_{c1}), \tag{4.1}$$

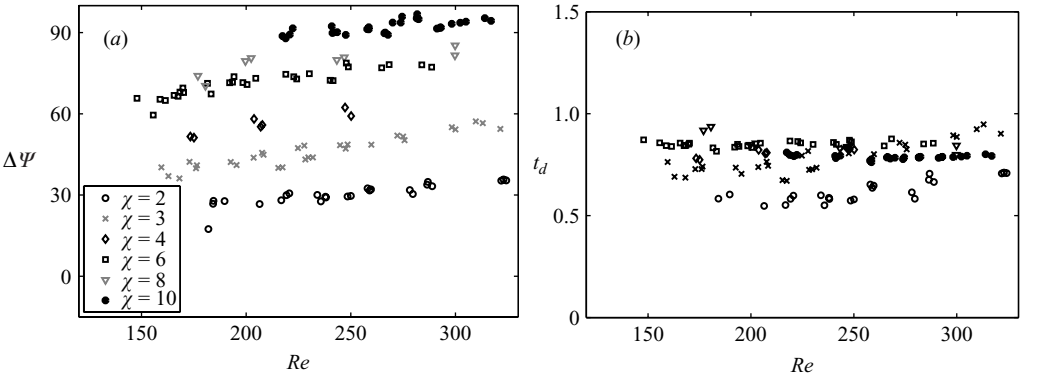

FIGURE 5. Phase difference between the transverse vortical force and the vortical torque as a function of the parameters χ and Re: (*a*) $\Delta\Psi$ (in degrees); (*b*) dimensionless time delay t_d.

$$v/S \approx 4.5 \times 10^{-2}\,(Re^* - Re^*_{c1})^{1/2} \sin(S\,t - \phi_Y), \tag{4.2}$$

$$\theta \approx 5.8 \times 10^{-2}(Re^* - Re^*_{c1})^{1/2} \sin(S\,t). \tag{4.3}$$

While these relations provide a central simplification to the problem, the phase difference ϕ_Y between the transverse velocity and the inclination remains a complicated function of both Re^* and χ (see figure 21 of Fernandes *et al.* 2007). Hence, the analysis of the kinematics did not lead us to a simple scaling of all the parameters of the body motion. As shown by Fernandes *et al.* (2005), ϕ_Y is important for the way the body motion evolves along its path: thick bodies move with their symmetry axis essentially aligned with the path, while thin bodies slide along the path with their symmetry axis perpendicular to it. In the previous section, we saw that ϕ_Y arises from the phase difference $\Delta\Psi = \phi(\Gamma^z_\omega) - \phi(F^y_\omega)$ between the vortical torque and the transverse vortical force. For all aspect ratios, the force F^y_ω is ahead of the torque Γ^z_ω and $\Delta\Psi$ changes by about 60° when the aspect ratio χ increases from 2 to 10 while it only weakly depends on Re, as shown in figure 5. $\Delta\Psi$ can also be expressed as a dimensionless time delay t_d scaled with the characteristic mean rise time t_o, through $t_d = \Delta\Psi/S$. As revealed by figure 5, t_d depends only weakly on the aspect ratio as well as on the Reynolds number. The time delay between the vortical torque and the transverse vortical force is thus of the order of t_o, whatever Re and χ.

Thus, two independent time scales appear to govern the problem. On the one hand, the oscillatory motion and vortex shedding occur with a period $T = f^{-1}$ proportional to d/u_1. On the other hand, the evolution of the vortex structure in the body wake, which governs the evolution of the vortical loads, depends on the time scale $t_o = d/u_o$ set by the mean rise motion. This view is supported by measurements of the fluid velocity in the wake performed with particle image velocimetry (Ern *et al.* 2007). It thus is also of interest to examine how the amplitudes of F^y_ω and Γ^z_ω scale with the two different gravitational velocities, u_o and u_1, and vary with Re^*. Two force scales can be naturally introduced: $f_o = \rho_f u_o^2 \pi d^2$ and $f_1 = \rho_f u_1^2 \pi d^2 = \chi f_o$. Figure 6 shows that a satisfactory collapse of the results, eliminating the dependence with respect to χ, is readily obtained for F^y_ω, indicating that f_o is the relevant scale for the vortical force. The transverse force F^y_ω therefore scales as the drag force F^x_ω and its phase relative to the body inclination angle θ is close to $-\pi/4$ for all aspect ratios, as shown by figure 4.

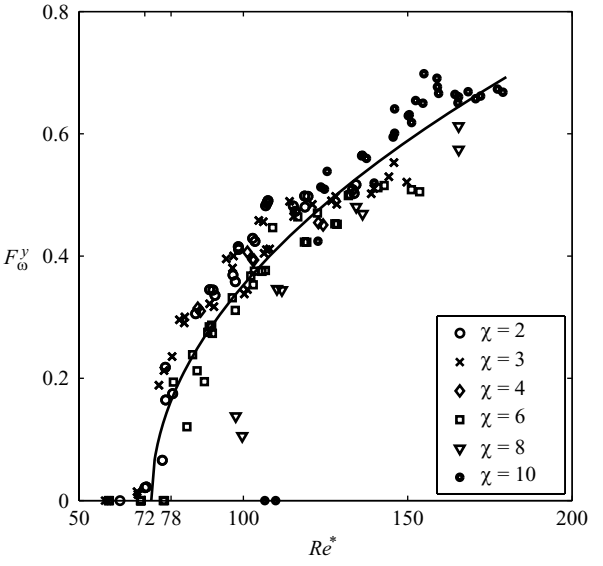

FIGURE 6. Evolution with Re^* of the amplitude of the transverse component of the vortical force F^y_ω. The line corresponds to the amplitude of the right-hand side of (4.7). The particular values 72 and 78 correspond to Re^*_{c1} and Re^*_{c2}, respectively.

The behaviour of the vortical torque is more complex, since neither the reference scale $\Gamma_o = f_o d$ alone nor the scale $\Gamma_1 = \chi\Gamma_o$ alone is capable of collapsing the measured amplitudes on a single master curve. This suggests that the vortical torque involves two contributions scaling respectively with Γ_o and Γ_1. The first of them is the torque Γ_f that results from the existence of the transverse force F^y_ω, namely

$$\Gamma_f = \alpha F^y_\omega(t + \phi_o/S) = \alpha\widetilde{F^y_\omega}\sin(St + \phi_o), \tag{4.4}$$

$\widetilde{F^y_\omega}$ denoting the amplitude of F^y_ω. It scales with Γ_o and we assume both its phase ϕ_o relative to F^y_ω and its lever arm α to be constant. We select $\alpha = 0.17$ (i.e. the dimensional lever arm is $0.17d$) and $\phi_o = \pi/18$, which are representative of values determined numerically for fixed bodies of aspect ratios $6 \leqslant \chi \leqslant 10$ in a uniform flow in the range of Reynolds numbers $200 \leqslant Re \leqslant 250$. The values of α and ϕ_o can be varied by 10% with negligible effect. The second contribution Γ_m accounts for the modification of the vortical torque due to the body oscillations and scales as Γ_1, namely

$$\Gamma_m = \beta\chi\sin(St - \phi_1). \tag{4.5}$$

The parameters $\beta(\chi, Re^*)$ and $\phi_1(\chi, Re^*)$ have been determined by equating the theoretical expression for the total vortical torque $\Gamma_m + \Gamma_f$ given by (4.4) and (4.5) with the measured vortical torque $\widetilde{\Gamma^z_\omega}\sin(St - \Delta\Psi)$. The corresponding results are plotted on figure 7. The amplitude is accurately fitted by choosing $\beta = \beta'(Re^* - Re^*_{c1})^{1/2}$ with $\beta' = 5.5 \times 10^{-3}$, while the phase ϕ_1 is found to be almost constant and close to $\pi/2$. It is remarkable that β is independent of χ and evolves with Re^* similarly to the transverse force, while ϕ_1 is independent of both Re^* and χ. This result provides a strong argument in favour of the relevance of the splitting assumption we made above for the vortical torque. With this result at hand, the characteristics of the vortical loads acting on all the bodies we considered can thus be described by the following

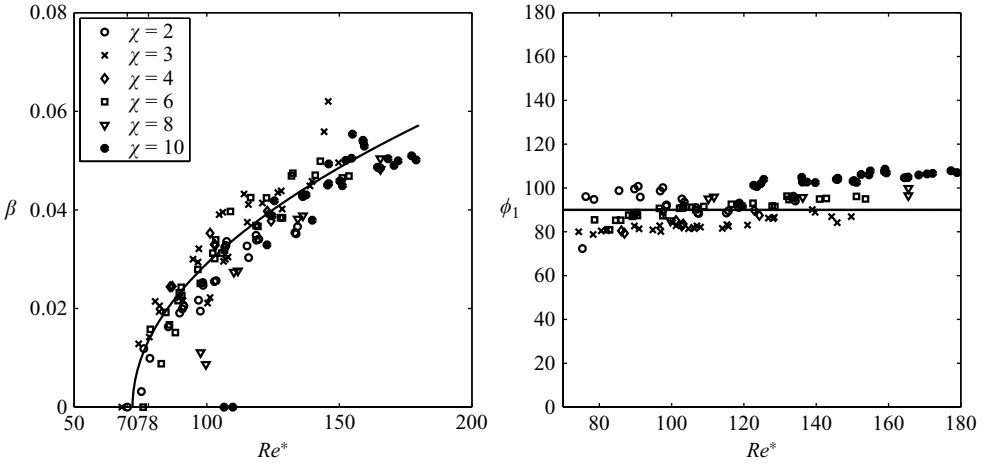

FIGURE 7. Evolution with Re^* of the amplitude parameter β and of the phase ϕ_1 defined in (4.5). The solid lines correspond to $\beta'(Re^* - Re^*_{c1})^{1/2}$ with $\beta' = 5.5 \times 10^{-3}$ and to $\phi_1 = \pi/2$, respectively.

analytical expressions:

$$F^x_\omega \approx -1, \tag{4.6}$$

$$F^y_\omega \approx -\frac{1}{15}(Re^* - Re^*_{c1})^{1/2} \sin(St), \tag{4.7}$$

$$\Gamma^z_\omega \approx -\frac{1}{200}(Re^* - Re^*_{c1})^{1/2} \left(34 \sin(St + \pi/18) + 11\chi \sin(St - \pi/2)\right), \tag{4.8}$$

where the origin of all phases is now defined relative to F^y_ω and the Strouhal number is $S \approx (\pi/5)\ \chi^{1/2}$. Figure 8 (resp. (6)) confirms that the amplitude of the vortical torque (resp. force) calculated from (4.8) (resp. (4.7)) compares well with the measured amplitude.

From the analysis of the onset of the wake instability for fixed bodies, we introduced the modified Reynolds number Re^* that accounts for the variation of vorticity production with the aspect ratio. Then, assuming that the body dynamics only involve the two gravitational velocity scales u_o and u_1 allowed us to express the dependence of the frequency, amplitudes and phases of F^y_ω and Γ^z_ω on χ and to show that the corresponding amplitudes are both proportional to $(Re^* - Re^*_{c1})^{1/2}$. The set of equations (4.6)–(4.8), which makes the dependence of the vortical loads on χ and Re^* explicit, is a first model of the vortical loads acting on a thick disk during its oscillatory motion. It is now interesting to consider whether the use of the vortical loads given by (4.6)–(4.8) could generate a motion that converges towards the fully developed zigzag when the body is released from rest. Solving the system (2.3)–(2.5) in terms of u, v and θ with the values of the vortical loads introduced as forcing terms can only provide the correct final solution if the initial conditions are the values of the desired solution (3.1) at $t = 0$. Otherwise, a solution corresponding to the homogeneous system, with no physical significance, also arises as part of the result (the proof is straightforward if the system is considered linear). We have observed that, when computed for a body released from rest, the high-frequency solution corresponding to the homogeneous system provides the main part of the complete solution. We know from experiments that for given χ and Re, the final trajectory of

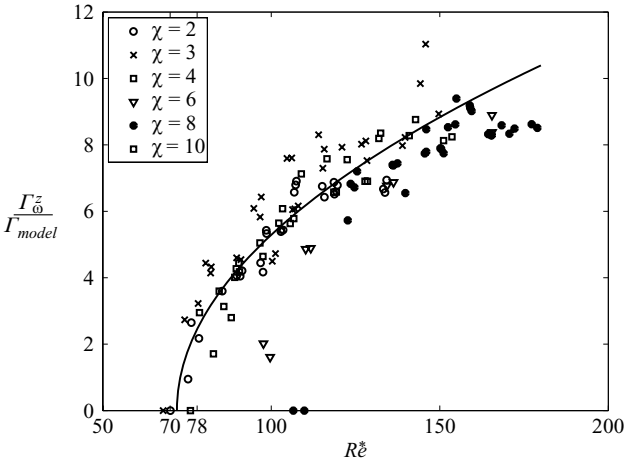

FIGURE 8. Evolution with Re^* of the amplitude of the vortical torque Γ^z_ω normalized by the amplitude Γ_{model} of the right-hand side of (4.8). The solid line corresponds to $(Re^* - Re^*_{c1})^{1/2}$.

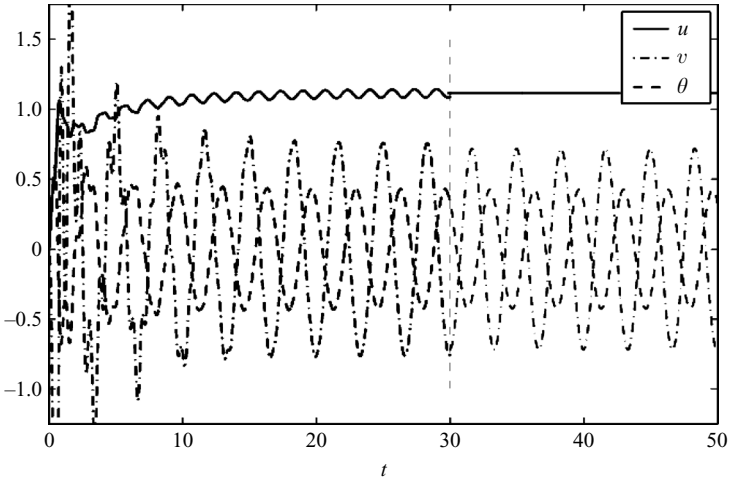

FIGURE 9. Comparison between the experimental characteristics of the path of a body and those determined by solving the system (2.3)–(2.5) forced by the model (4.6)–(4.8) of the vortical loads supplemented with a damping term ($\chi = 10$, $Re = 250$). For $t \leqslant 30$ the curves correspond to the numerical solution obtained with damping coefficients $C_v = 0$, $C_r = 0.016$; initial conditions are $u = v = r = 0$ and $\theta = 1°$. For $t \geqslant 30$, the curves correspond to experimental results; the origin of time was adjusted to match the numerical results at $t = 30$.

the body characterized by u, v and θ is unique, independent of the initial conditions (i.e. the angle and velocity of release of the body in the tank). To converge towards the physical solution, a possibility is then that the expressions for the vortical force and torque include terms capable of damping the eigenmodes of the homogeneous system.

An heuristic attempt in this direction was made by adding the damping terms $F^y_{\omega d} = -C_v \overline{u} v$ and $\Gamma^z_{\omega d} = -C_r |r| r$ to the transverse force equation (2.4) and the torque

equation (2.5), respectively. Using the sinusoidal signals $F_\omega^y(t)$ and $\Gamma_\omega^z(t)$ provided by (4.6)–(4.8), the system was then forced with the loads $F_{\omega nd}^y = F_\omega^y - F_{\omega d}^y$ and $\Gamma_{\omega nd}^z = \Gamma_\omega^z - \Gamma_{\omega d}^z$. Solving for $\chi = 2$ and 10 yielded the desired solution for various sets of initial conditions after the values of the coefficients C_v and C_r were properly tuned. For $\chi = 10$, the required damping terms were found to be very small, namely $F_{\omega d}^y = 0$ and $\Gamma_{\omega d}^z$ was less than one percent of Γ_ω^z. Figure 9 shows the kinematic characteristics of the corresponding simulated motion for $t \leqslant 30$, the simulation starting from rest. The experimental result is also displayed for $t \geqslant 30$. It clearly appears that, provided such a small damping is included, the dynamical system forced by the harmonic expression for the vortical loads converges towards a stable asymptotic solution in good agreement with the measured motion. This result confirms that the expression for the vortical loads given by (4.6)–(4.8) can be safely used as a forcing term to compute the motion of freely moving bodies and to guide the elaboration of more satisfactory theoretical models in which the explicit dependence on time is removed.

5. Conclusions

We have investigated the force and torque balances governing the planar zigzag motion of rigid, freely moving thick disks in the aspect ratio range $2 < \chi < 10$, $100 < Re < 330$, for a density ratio $\rho_s/\rho_f \simeq 1$. We found that the body oscillatory behaviour is essentially governed by the force balance along the body transverse direction and by the torque balance: the vortical force is mainly balanced by the inertia force generated by the body rotation and by the transverse buoyancy component, while the vortical torque is mainly balanced by the restoring added-mass torque. Both linear and angular accelerations provide only secondary contributions to these balances. The present investigation also revealed that the evolution of the inertia forces with the aspect ratio cannot be anticipated on the sole grounds of the evolution of the proper- and added-inertia coefficients. The aspect ratio strongly influences the characteristics of the unsteady wake and, as a consequence, the body motion. In particular, the phase difference between the vortical force and torque, which increases continuously with the aspect ratio, appears to be responsible for the phase difference between the body velocity and orientation.

The key motivation for the present work was to provide results that can guide the elaboration of dynamical models capable of predicting quantitatively the oscillatory paths of non-spherical bodies. A first step towards this objective was achieved by identifying the characteristic scales for the amplitude and phase of the vortical contributions. More precisely, the transverse vortical force was found to be proportional to the buoyancy force f_0 acting on the body, whereas the vortical torque was found to be the sum of two contributions, one scaling as $f_o d$ and another one scaling as $\chi f_o d$. The corresponding normalized amplitudes and phases of the vortical loads are independent of the aspect ratio but their amplitudes depend on the Reynolds number through a square-root law of the form $(Re/Re_{c1} - 1)^{1/2}$, where Re_{c1} is the threshold of the first instability of the wake behind the corresponding body held fixed in a uniform stream. Since the present data only cover the developed state of the motion, the explicit, harmonic, time dependence of the vortical loads could not be removed. The next step of our research will be to consider the initial transient in order to remove this explicit dependence by examining how the wake-induced force and torque can be related unambiguously to the history of the velocity and acceleration of the body.

REFERENCES

Andersen, A., Pesavento, U. & Wang, Z. J. 2005 Unsteady aerodynamics of fluttering and tumbling plates. *J. Fluid. Mech.* **541**, 65–90.

Ern, P., Fernandes, P. C., Risso, F. & Magnaudet, J. 2007 Evolution of the wake structure and wake-induced loads along the path of freely rising axisymmetric bodies. *Phys. Fluids* **19**, 113302.

Fernandes, P. C., Ern, P., Risso, F. & Magnaudet, J. 2005 On the zigzag dynamics of freely moving axisymmetric bodies. *Phys. Fluids* **17**, 098107.

Fernandes, P. C., Risso, F., Ern, P. & Magnaudet, J. 2007 Oscillatory motion and wake instability of freely-rising axisymmetric bodies. *J. Fluid Mech.* **573**, 479–502.

Howe, M. 1995 On the force and moment on a body in an incompressible fluid, with application to rigid bodies and bubbles at low and high Reynolds numbers. *Q. J. Mech. Appl. Maths* **48**, 401–426.

Lamb, H. 1932 *Hydrodynamics*, 6th edn. Cambridge University Press.

Loewenberg, M. 1993*a* Stokes resistance, added mass, and Basset force for arbitrarily oriented finite-length cylinders. *Phys. Fluids* A **5**, 765–767.

Loewenberg, M. 1993*b* The unsteady Stokes resistance of arbitrarily oriented, finite-length cylinders. *Phys. Fluids* A **5**, 3004–3006.

Loewenberg, M. 1994 Asymmetric, oscillatory motion of a finite-length cylinder: the macroscopic effect of particle edges. *Phys. Fluids* **6**, 1095–1107.

Lugt, H. J. 1983 Autorotation. *Annu. Rev. Fluid. Mech.* **15**, 123–147.

Magnaudet, J. & Eames, I. 2000 The motion of high-Reynolds-number bubbles in inhomogeneous flows. *Annu. Rev. Fluid Mech.* **32**, 659–708.

Mougin, G. & Magnaudet, J. 2002*a* The generalized Kirchhoff equations and their application to the interaction between a rigid body and an arbitrary time-dependent viscous flow. *Intl J. Multiphase Flow* **28**, 1837–1851.

Mougin, G. & Magnaudet, J. 2002*b* Path instability of a rising bubble. *Phys. Rev. Lett.* **88**, 014502.

Mougin, G. & Magnaudet, J. 2006 Wake-induced forces and torques on a zigzagging/spiralling bubble. *J. Fluid Mech.* **567**, 185–194.

Shew, W., Poncet, S. & Pinton, J.-F. 2006 Force measurements on rising bubbles. *J. Fluid Mech.* **569**, 51–60.

Wang, Z. J. 2005 Dissecting insect flight. *Annu. Rev. Fluid Mech.* **37**, 183–210.